

Helium Variation Across Two Solar Cycles Reveals A Speed-Dependent Phase Lag

B. L. ALTERMAN^{1,2} AND JUSTIN C. KASPER^{2,3}

¹*University of Michigan
Department of Applied Physics
450 Church St.*

Ann Arbor, MI 48109, USA

²*University of Michigan*

*Department of Climate & Space Sciences & Engineering
2455 Hayward St.*

Ann Arbor, MI 48109-2143, USA

³*Smithsonian Astrophysical Observatory*

*Observatory Building E
60 Garden St.*

Cambridge, MA 02138, USA

ABSTRACT

We study the relationship between solar wind helium to hydrogen abundance ratio (A_{He}), solar wind speed (v_{sw}), and sunspot number (SSN) over solar cycles 23 and 24. This is the first full 22-year Hale cycle measured with the *Wind* spacecraft covering a full cycle of the solar dynamo with two polarity reversals. While previous studies have established a strong correlation between A_{He} and SSN, we show that the phase delay between A_{He} and SSN is a monotonic increasing function of v_{sw} . Correcting for this lag, A_{He} returns to the same value at a given SSN over all rising and falling phases and across solar wind speeds. We infer that this speed-dependent lag is a consequence of the mechanism that depletes slow wind A_{He} from its fast wind value during solar wind formation.

Keywords: solar wind, sunspots, Sun: abundances, acceleration of particles, interplanetary medium, Sun: fundamental parameters

1. INTRODUCTION

Fully ionized hydrogen or protons (p) and fully ionized helium or alpha particles (He or α) are the two most abundant solar wind ion species. The former comprises $\sim 95\%$ of the solar wind ions and the latter $\sim 4\%$, both by number density. Heavier, minor ions constitute the remaining. The alpha particle abundance ($A_{\text{He}} = 100 \times n_{\alpha}/n_p$) strongly correlates with solar activity, as indicated by the sunspot number (SSN) (Aellig et al. 2001; Kasper et al. 2007, 2012). The cross correlation and slope between A_{He} and SSN varies with solar wind speed (v_{sw}); is strongest in slow wind; markedly falls off above $v_{\text{sw}} = 426 \text{ km s}^{-1}$, where A_{He} takes on a stable value between 4% and 5%; and vanishes in the solar wind for speeds below $v_0 = 259 \text{ km s}^{-1}$ (Kasper et al.

2007, 2012). This helium vanishing speed is within 1σ of the minimum observed solar wind speed (Kasper et al. 2007), indicating that helium may be essential to solar wind formation in the corona.

In addition to SSN, many other indicators of solar activity also follow a similar ~ 11 year cycle (Ramesh & Vasantharaju 2014) that demonstrate a distinct phase-offset with SSN, which has been referred to as a hysteresis-like effect. These offsets range from 30 days (Bachmann & White 1994) to 450 days (Temmer et al. 2003). Goelzer et al. (2013) have shown a similar phase lag in the interplanetary magnetic field's response to changes in SSN.

Using observations from the *Wind* Faraday cups (FC), we extend the study of A_{He} variation with SSN and v_{sw} by Kasper et al. (2007, 2012) to include more than 23 years. This time period encompasses solar cycles 23 and 24 along with the end of solar cycle 22, thereby covering one Hale cycle. In other words, an idealized sun with a pure dipole magnetic field would have experienced two

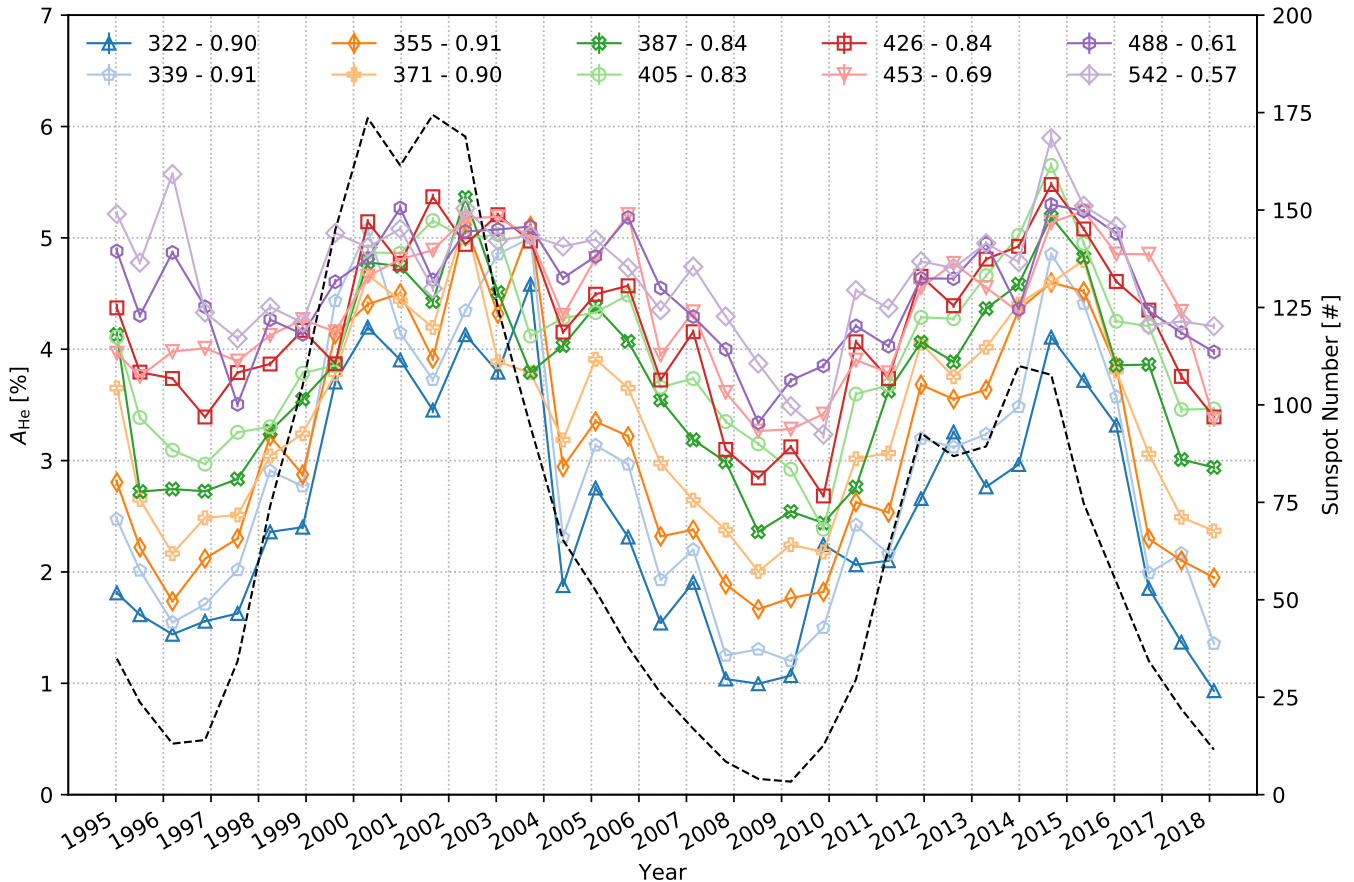


Figure 1. Helium abundance (A_{He}) as a function of time and solar wind speed. Solar wind speed (v_{sw}) is divided into ten quantiles. Thirteen month smoothed SIDC Sunspot Number (SSN, dashed black) is plotted on the secondary y-axis. The legend indicates the middle of a given v_{sw} quantile and the Spearman rank correlation coefficient between A_{He} and SSN for that quantile. In effect, this figure updates Fig. (1) of Kasper et al. (2007, 2012). The present drop in A_{He} reflects the onset of solar minimum 25.

polarity reversals and be returning to the configuration it had at the end of cycle 22.

In this work, we expand on the results of Kasper et al. (2007, 2012). We show a positive correlation between A_{He} and SSN across multiple solar cycles. In the slowest wind, we find a characteristic A_{He} that is consistent across multiple minima and maxima. Examining this relationship over one Hale cycle, we demonstrate that the phase lag between A_{He} and SSN found by Feldman et al. (1978) is a monotonically increasing function of v_{sw} . This delay is characteristic to a given v_{sw} and, at any one v_{sw} , a cyclic delay is sufficient to correct for this lag. Unexpectedly, A_{He} returns to similar values in both maximum 23 and maximum 24 even though $\text{SSN}_{\text{Max},24} < \text{SSN}_{\text{Max},23}$. Our results are consistent when using the 13-month smoothed, monthly, and daily sunspot numbers.

The remainder of this Letter is dedicated to analyzing and interpreting this speed-dependent lag. Section 2 describes the observations and FC specifics that are

key to this study. Section 3 describes the variation of A_{He} with v_{sw} and SSN over two solar cycles. Section 4 analyzes the delay in response of A_{He} to changes in SSN as a function of v_{sw} . Section 5 presents the relationship between A_{He} and SSN in various v_{sw} quantiles, corrected for the delay of peak cross-correlation coefficient. Here, we show that correcting for the lag in A_{He} 's response to changes in SSN reduces this hysteresis effect to a linear relationship. In Section 6, we use A_{He} 's dependence on SSN to investigate the robustness of the A_{He} , v_{sw} , SSN relationship reported by Kasper et al. (2007). In Section 7, we interpret our results and extend earlier hypotheses regarding two sources of slow solar wind. Finally, Section 8 summarizes these results and discusses future work.

2. DATA SOURCES

The *Wind* spacecraft has been in continuous operation since its launch in the fall of 1994. Ogilvie et al. (1995) provide a detailed description of the Solar Wind

Experiment (SWE) Faraday cups (FC). Kasper et al. (2006) introduce techniques for optimizing the algorithms that extract physical quantities from FC measurements. Maruca & Kasper (2013) and Alterman et al. (2018) build on these algorithms. These data have resulted in high precision solar wind measurements of alpha particles (Kasper et al. 2006; Maruca & Kasper 2013) and multiple proton populations (Alterman et al. 2018). The FC ion distributions are available on CDAweb¹ and SPDF². We follow Alterman et al. (2018) and reprocess the raw measurements to extract two proton populations (core and beam) along with an alpha particle population. The proton core is the population with the larger of the two proton densities. We calculate the solar wind speed as the proton center-of-mass velocity and treat the proton core as the proton density when calculating A_{He} .

Two aspects of FCs are key to this work. First, FCs are energy-per-charge detectors. In the highly supersonic solar wind, alpha particles and protons are well separated by the instrument even when they are co-moving (Kasper et al. 2008, 2017; Alterman et al. 2018), as is commonly the case in slow solar wind. Second, the measurement quality has been stable and accurate throughout the mission (Kasper et al. 2006). These two FC characteristics enable our study of A_{He} variation with a single dataset from one instrument suite covering the 23 years necessary to observe one Hale cycle.

3. SOLAR CYCLE VARIATION

Fig. 1 presents A_{He} as a function of v_{sw} and time over 23 years. This time period starts at the trailing end of cycle 22 and extends through the declining phase of cycle 24. Fig. 1 follows the format of Kasper et al. (2007, 2012, Figure (1) in each) and can be considered an update to their results. The solar wind speed measurements from the full mission have been split into 12 quantiles. The fastest and slowest quantile have been discarded due to measurement and statistical considerations. Of those quantiles retained, the lower edge of the slowest is 312 km s^{-1} and the upper edge of the fastest is 574 km s^{-1} . Consequently, this study is limited to solar wind typically categorized as slow or slow and intermediate speed.³ As in prior work, the abundance in each v_{sw} quantile is averaged into 250 day intervals.

The 13-month smoothed sunspot number (SILSO World Data Center 2018; Vanlommel et al. 2005, SSN) is interpolated to the measurement time; averaged into the same 250 day intervals as A_{He} ; and plotted on the secondary y-axis. The legend indicates the middle of the solar wind speed quantile along with its corresponding Spearman rank cross correlation coefficient between A_{He} and SSN. For brevity, we henceforth indicate the Spearman rank cross-correlation coefficient between A_{He} and SSN as $\rho(A_{\text{He}}, \text{SSN})$.

Fig. 1 indicates that $\rho(A_{\text{He}}, \text{SSN})$ peaks at $v_{\text{sw}} = 355 \text{ km s}^{-1}$. The present drop in A_{He} reflects that the sun is entering Minimum 25. In contrast to the results of Kasper et al. (2007, 2012), $\rho(A_{\text{He}}, \text{SSN}) > 0.6$ indicates a meaningful cross-correlation in all but the fastest reported quantile with $v_{\text{sw}} = 542 \text{ km s}^{-1}$ and $\rho(A_{\text{He}}, \text{SSN}) \geq 0.7$ is highly significant up to $v_{\text{sw}} = 426 \text{ km s}^{-1}$. As Feldman et al. (1978) noted, there is a phase offset between A_{He} and $\rho(A_{\text{He}}, \text{SSN})$. Although the cycle 23 SSN amplitude is less than the cycle 24 amplitude, A_{He} unexpectedly returns to comparable values during each maximum.

4. TIME-LAGGED CROSS CORRELATION

Visual inspection indicates a clear time lag between A_{He} and SSN. To quantify this lag, we calculate $\rho(A_{\text{He}}, \text{SSN})$ as a function of delay time applied to SSN from -200 days to $+600$ days in steps of 40 days—slightly longer than one solar rotation—for each v_{sw} quantile. We smooth these results to reduce the impact of discretization. The delay time is the time for which $\rho(A_{\text{He}}, \text{SSN})$ peaks as a function of delay. Panel (a) of Fig. 2 plots the peak cross correlation coefficient as a function of v_{sw} for observed (empty marker) and delayed (filled marker) SSN. Marker colors and symbols match Fig. 1 and are maintained throughout the Letter. Dotted lines connect the markers to aid the eye. To estimate the error in this calculation and its sensitivity to averaging timescale, we repeated it for averaging windows $N_{\text{days}} = 225$ to $N_{\text{days}} = 275$ in steps of 5 days. Because a trend is not apparent, we choose to quantify this variability as the standard deviation across N_{days} and represent it as error bars centered on the $N_{\text{days}} = 250$ averaging window utilized in this Letter.

Several features in Panel (a) of Fig. 2 stand out. First, it emphasizes that delayed $\rho(A_{\text{He}}, \text{SSN}) \geq 0.7$ is highly correlated for all v_{sw} quantiles. Second, observed and delayed $\rho(A_{\text{He}}, \text{SSN})$ peak at the same $v_{\text{sw}} = 355 \text{ km s}^{-1}$. Third, the change in $\rho(A_{\text{He}}, \text{SSN})$ is largest and most visually striking in faster wind. However, smaller changes in slower wind's $\rho(A_{\text{He}}, \text{SSN})$ are sta-

¹ https://cdaweb.sci.gsfc.nasa.gov/misc/NotesW.html#WLSW-ION-DIST_SWE-FARADAY

² ftp://spdf.gsfc.nasa.gov/pub/data/wind/swe/swe_faraday/

³ To be consistent with prior work (e.g. Kasper et al. (2007, 2012)), we will use *slow* and *fast* to refer to the different extremes presented here. However, the reader should know that truly fast solar wind is excluded from our study.

tistically more significant because they are less likely to be due to random fluctuations.

Panel (b) of Fig. 2 examines τ , the delay of peak $\rho(A_{\text{He}}, \text{SSN})$, as a function of v_{sw} . A positive delay indicates that changes in SSN precede changes in A_{He} . The insert at the top of the figure indicates the functional form, fit parameters, and quality metrics. As with Panel (a) of Fig. 2, the error bars indicate the variability of τ in each v_{sw} quantile. Solving the fit equation for $\tau = 0$, or the speed at which A_{He} responds immediately to changes in SSN, results in $v_i = 200 \text{ km s}^{-1}$. Nevertheless, it is not unambiguously clear if delay time τ monotonically increases with v_{sw} or there are two distinct delay times. If it is actually the latter, then A_{He} in slow wind responds to changes in SSN with a delay time $\tau_{\text{slow}} = 150$ days; faster wind responds after $\tau_{\text{fast}} > 300$ days; and v_i represents a non-trivial conflation of these two delays. If this is not the case, it may be that τ_{slow} is the shortest delay with which A_{He} responds to changes in SSN. As discussed below, in either case all helium released into the solar wind still lags changes in SSN.

5. PHASE DELAY

Fig. 3 presents A_{He} as a function of SSN in the example quantile $v_{\text{sw}} = 355 \text{ km s}^{-1}$. This is the v_{sw} quantile for which the change in cross-correlation coefficient $\Delta\rho(A_{\text{He}}, \text{SSN})$ is smallest and the phase delay's effect is least likely to be due to random fluctuations. Panel (a) uses the observed SSN. Panel (b) uses SSN delayed by the time indicated in Panel (b) of Fig. 2, ~ 150 days. A line connects the points to aid the eye. Both line and marker color indicate the days since mission start, given by the color bars. Marker shapes match the style of previous figures. Both panels contain a robust fit to the data, each indicating the monotonic, increasing trend. As in Panel (b) of Fig. 2, the insert at the top of each panel describes the fit.

Panel (a) clearly shows the hysteresis pattern of A_{He} as a function of SSN. As seen with other indices (e.g. Bachmann & White (1994)), time moves counter-clockwise in this plot.⁴ As noted by Bachmann & White (1994) for several solar indices, the clustering of data at small SSN indicates that the hysteresis effect is stronger at solar maximum and weaker at solar minimum.

In panel (b), the larger R^2 indicates that this spread of A_{He} about the trend decreases. Note that R^2 cor-

⁴ Not all indices present with the same handedness and the handedness of some changes across solar cycles (Özgüç & Ataç 2001). A larger study of A_{He} variation is necessary to generalize this handedness observation.

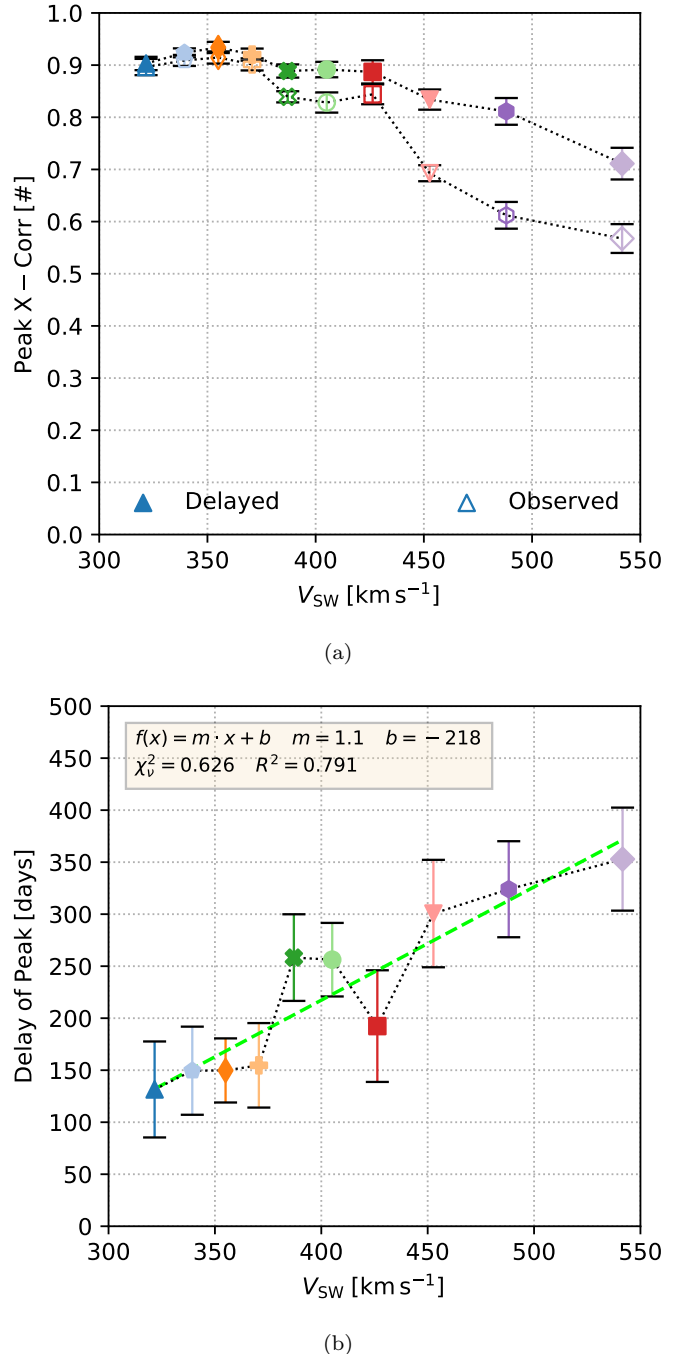


Figure 2. Plots characterizing the cross correlation coefficient as a function of solar wind speed (v_{sw}) for the observed (empty markers) and delayed (filled markers) SSN using 250 day averages. The marker color and shape match the style of Fig. 1. Dotted lines connect the markers to aid the eye. Panels are: (a) Spearman rank cross-correlation coefficient and (b) Delay (τ) of Peak Spearman rank cross correlation as a function of v_{sw} . In (b), the dashed green line indicates a robust fit and the panel's insert provides the functional form, fit parameters, and quality metrics. A positive delay indicates that changes in SSN precede changes in A_{He} .

responds to the square of the correlation coefficient of A_{He} and SSN derived from a robust fit and not directly from the measurements. *Although R is similar to $\rho(A_{\text{He}}, \text{SSN})$, they are not trivially equal.* That delayed χ^2_{ν} is markedly closer to unity indicates that a linear model better characterizes A_{He} as a function of delayed rather than observed SSN. Because delayed SSN only reduces the spread of A_{He} about the trend, it is expected that the trends and fit parameters in both cases are similar.

6. ROBUSTNESS OF $A_{\text{He}}(V)$

Kasper et al. (2007) describe the relationship between A_{He} and v_{sw} in slow wind ($v_{\text{sw}} \leq 530 \text{ km s}^{-1}$) using data from a 2 year interval surrounding solar Minimum 23. They find that $A_{\text{He}}(v) = 1.63 \times 10^{-2} (v - v_0)$, where $v_0 = 259 \pm 12 \text{ km s}^{-1}$ is the speed below which helium vanishes from the solar wind. The robust fits in Fig. 3 allow us to extract A_{He} at zero solar activity for all v_{sw} quantiles. This quantity, $A_{\text{He}}(\text{SSN} = 0)$, represents low solar activity conditions across this Hale cycle that are appropriate for comparison to the minimum 23 results from Kasper et al. (2007).

Fig. 4 plots $A_{\text{He}}(\text{SSN} = 0)$ in all v_{sw} quantiles for delayed SSN with unfilled markers. As observed SSN does not deviate from delayed SSN in this figure, it is omitted for clarity. The black dashed curve is the fit of $A_{\text{He}}(v)$ from Kasper et al. (2007). To better compare this analysis to the work of Kasper et al. (2007), filled markers present the results of repeating this analysis for $\text{SSN} < 25$, a range in SSN representative of solar minimum 23. That $A_{\text{He}}(\text{SSN} = 0)$ is smaller in this reanalysis using a restricted range of SSN further substantiates that our results are consistent with those of Kasper et al. (2007) even though ours cover multiple solar cycles, a larger range in solar activity conditions, and uses a different analysis technique. Furthermore, the agreement between these two distinct analysis techniques supports the interpretation that helium release is essential to solar wind formation (Kasper et al. 2007). The discrepancy between our fastest quantile with $v_{\text{sw}} = 542 \text{ km s}^{-1}$ and their trend is expected because (1) it is outside of the speed range they fit and (2) they found that A_{He} at this and similarly high speeds takes on a stable value between 4% and 5%.

7. HELIUM FILTRATION

Many solar indices have a distinct phase-offset or hysteresis-like behavior with SSN (Ramesh & Vasantharaju 2014, and references therein). Two such indicators include Lyman- α ($L\alpha$) intensity and soft x-ray flux (SXR). $L\alpha$ measures activity in the sun's chromosphere & transition region (Fontenla et al. 2001, 1988)

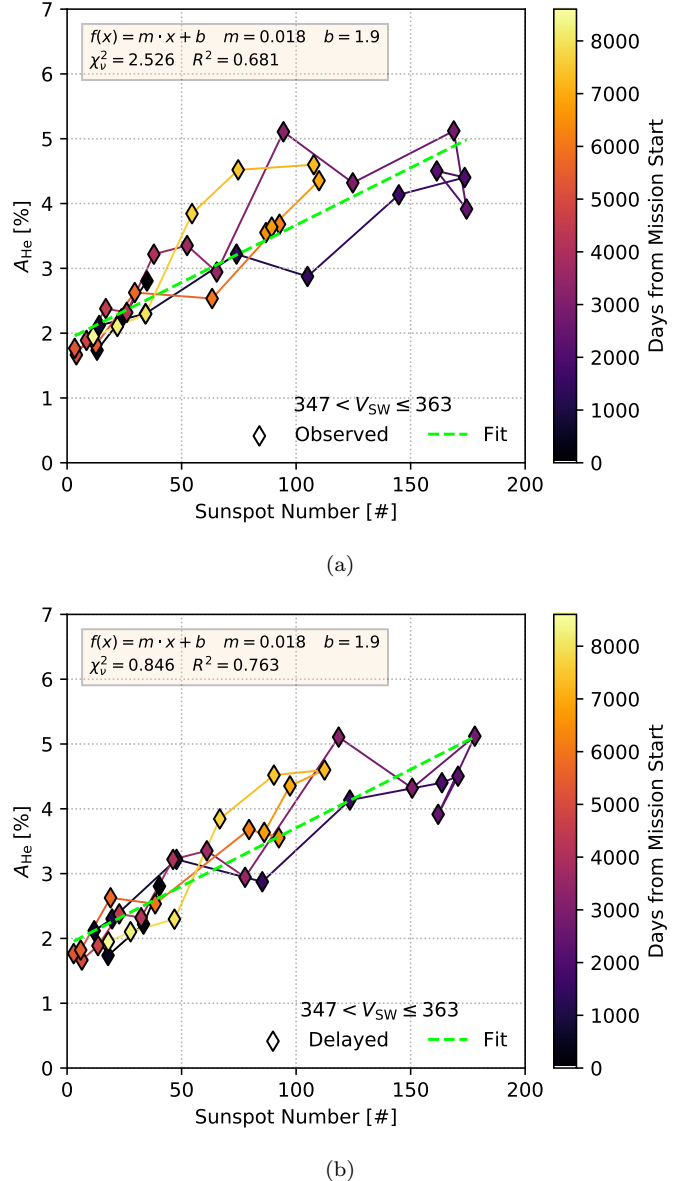


Figure 3. Helium abundance (A_{He}) as a function of (a) observed and (b) delayed SSN in one example v_{sw} quantile. A line connects the points to aid the eye. Line and marker color correspond to the number of days since mission start. Marker shape matches the quantile in previous figures. This v_{sw} quantile covers the range $347 \text{ km s}^{-1} < v_{\text{sw}} \leq 363 \text{ km s}^{-1}$. A green, dashed line presents a robust fit to each trend. The insert at top of each panel gives the function fit, fit parameters, and quality metrics. Delaying SSN by the phase offset appropriate to this v_{sw} quantile reduces the impact of the hysteresis effect, as the increase in delayed R^2 indicates. That χ^2_{ν} is closer to unity in (b) indicates that a linear model better describes A_{He} as a function of delayed SSN.

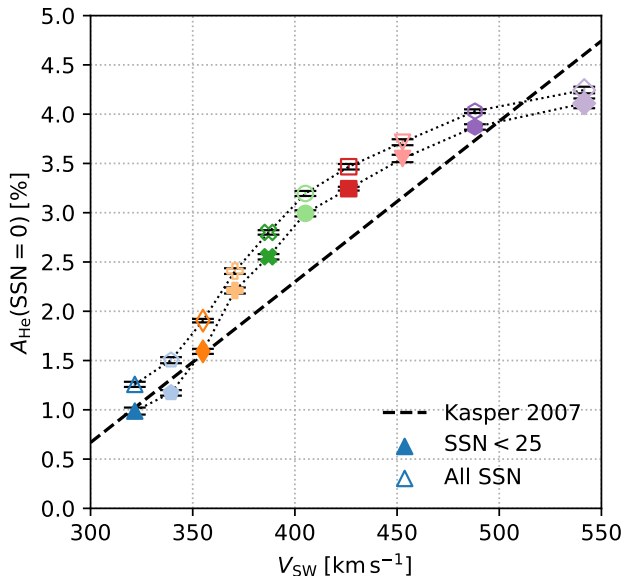


Figure 4. A summary of the zero solar activity helium abundance, $A_{He}(SSN = 0)$, as a function of v_{sw} for all robust fits in the fashion of Fig. 3. Error bars indicate the standard deviation of each quantity over the range in averaging windows $225 \leq N_{days} \leq 275$, each centered on the $N_{days} = 250$ value. Unfilled markers show all SSN. Filled markers show identical calculations with $SSN < 25$. The black dashed curve is the relationship between A_{He} and SSN derived by Kasper et al. (2007). That repeating our calculation with a reduced range in SSN shows better agreement with the results of Kasper et al. (2007) indicates that our results, covering the full range of solar activity in cycles 23 and 24, are consistent with their results from the two year interval surrounding minimum 23.

and lags SSN by 125 days (Bachmann & White 1994). SXR is most common in Active Regions (AR) (van Driel-Gesztelyi & Green 2015), and lags SSN by 300 days to 450 days (Temmer et al. 2003).

While A_{He} is approximately 8.5% within the sun’s convection zone and out to the photosphere (Asplund et al. 2009; Laming 2015), it rarely exceeds 5% in the corona (Laming & Feldman 2003; Mauas et al. 2005). It has long been assumed that A_{He} is initially modified in the photosphere. However, the speed-dependent lag in A_{He} ’s response to changes in SSN found here suggests additional processes at higher altitudes further modify helium’s abundance. Slow solar wind’s 150 day lag tracks lags in transition region and chromosphere structures, while faster wind’s 300 day lag is more consistent with higher altitude structures in the corona. How could the transition region or corona modify the helium abundance?

Kasper et al. (2007) propose that two mechanisms release fully ionized helium into the slow solar wind, one

each in the streamer belt and ARs. ARs have a strong magnetic field that extends from the photosphere into the corona, originate well above the equatorial region, tend to migrate towards the equator as they get older, and have loops that tend to grow with age (van Driel-Gesztelyi & Green 2015). In contrast, the streamer belt has a weaker magnetic field, is composed of loops larger than those typical of ARs, is magnetically closed to the heliosphere, and is typically considered the source of slow solar wind (Eselevich & Eselevich 2006). Stakhiv et al. (2016) identify signatures of these two solar sources in ACE/SWICS composition measurements.

If there are two sources of slow wind, solar wind originating in the streamer belt is more processed than that originating in ARs, where SXR is enhanced. Slower wind A_{He} ($v_{sw} < 375$ km s⁻¹) originates from the streamer belt with a phase delay $\tau_{slow} = 150$ days. It appears more depleted than faster solar wind from ARs that has a phase delay $\tau_{fast} > 300$ days. The magnitude of A_{He} ’s reduction from its photospheric value and the speed-dependent delay then reflect the extent to which a given source region is magnetically open to the heliosphere. As the phase delay between A_{He} and SSN is an increasing function of v_{sw} , ARs and the streamer belt may be two extreme cases along the continuum of slow wind helium depletion mechanisms.

For illustrative purposes, one candidate mechanism that may contribute to this processing is the FIP effect. The FIP effect is the empirical observation that solar wind ions are fractionated, or their abundances differ from their photospheric value based on their first ionization potential (Meyer 1991, 1993; Laming 2015, and references therein). Low FIP elements (FIP < 10 eV) tend to increase or experience an enhancement. This low-FIP enhancement also leads to an apparent depletion in high-FIP elements, as with helium. Under the framework of Rakowski & Laming (2012), time averaged coronal Alfvén waves create a ponderomotive force that accelerates ions into the corona and leads to fractionation in coronal loops. The FIP effect is strongest in the upper chromosphere and lower transition region, weakest in regions of strong magnetic field, and stronger in longer loops (Rakowski & Laming 2012). Feldman et al. (2005) found that FIP bias in ARs increases with age.

However, this is just one of several possible mechanisms that could cause this phase lag. Other mechanisms that might impact the speed-dependent phase lag may include interchange reconnection (Fisk 2003) and gravitational settling (Hirshberg 1973; Borrini et al. 1981; Vaclair & Charbonnel 1991). Moreover, these are mechanisms that are not mutually exclusive. Schwadron et al. (1999); Laming (2004); Rakowski & Laming (2012)

include gravitational settling in their models of the FIP effect. Schwadron et al. (1999) also relies on interchange reconnection to create the magnetic structures necessary for FIP fractionation to occur. As Rakowski & Laming (2012) show, the combination of coronal loop length, differences in gravitational scale height, and the FIP effect can lead to the apparent depletion of A_{He} . Whatever the underlying mechanism, it should also account for the observation that A_{He} returns to a similar value during solar maximum, irrespective of SSN during maximum.

8. CONCLUSION

Following the methods of Kasper et al. (2007, 2012), we have analyzed the relationship between A_{He} and the 13-month smoothed sunspot number (SSN) by studying their cross correlation coefficient using 250 day averages. We have verified that our results are consistent when using the monthly and daily SSN. Our data covers 23 years, including cycle 23 and 24 along with the tail end of cycle 22. This time period is more than the 22 years of a Hale cycle over which the pure dipole field of an idealized sun would experience two polarity reversals and return to an initial configuration. As shown in Fig. 1, the present decrease in A_{He} clearly demonstrates that we are entering solar Minimum 25. While the significance of the cross correlation coefficient $\rho(A_{\text{He}}, \text{SSN})$ decreases with increasing v_{sw} , Fig. 1 shows that $\rho(A_{\text{He}}, \text{SSN})$ is meaningful up to $v_{\text{sw}} = 488 \text{ km s}^{-1}$ and highly significant up to $v_{\text{sw}} = 426 \text{ km s}^{-1}$. A subject of future work is investigating why A_{He} returns to a similar value in Maximum 24 even though cycle 24's amplitude is markedly smaller than cycle 23's.

Feldman et al. (1978) comment on a phase offset between A_{He} and SSN. Panel (b) of Fig. 2 reveals that (1) the length of this delay is an increasing function of v_{sw} and (2) the v_{sw} quantile most correlated with SSN does not change when SSN is appropriately delayed in each quantile. We have also argued that, although changes in $\rho(A_{\text{He}}, \text{SSN})$ are most dramatic in faster v_{sw} quantiles, the probability of smaller changes in slower wind's larger $\rho(A_{\text{He}}, \text{SSN})$ is much smaller and therefore more significant.

Panel (b) of Fig. 2 presents the delay applied to SSN necessary to maximize $\rho(A_{\text{He}}, \text{SSN})$ as a function of v_{sw} . The delay is a monotonically increasing function of v_{sw} and linear fit to this trend reveals that the speed at which A_{He} responds instantaneously to changes in SSN is $v_i = 200 \text{ km s}^{-1}$. Yet the speed of instantaneous response is less than the vanishing speed, $v_i < v_0$. Therefore any helium released into the solar wind will necessarily response to changes in SSN after some delay. If trend in Panel (b) of Fig. 2 is correct, then the mini-

mum delay in A_{He} 's response to SSN is 68 ± 13 days, or approximately two Carrington Rotations. Here, we also note that there may be two distinct phase delays (τ_{slow} and τ_{fast}) with which A_{He} responds to changes in SSN and the fit quantity v_i may be a conflation of the physics related to each phase delay. Under either interpretation, helium released into the solar wind is a delayed response to changes in SSN.

In Section 5, we present robust fits to A_{He} as a function of observed and delayed SSN in each v_{sw} quantile. It visually illustrates that applying a time delay to SSN reduces the spread of A_{He} about its trend. In Section 6, we use helium abundance at zero solar activity derived from these fits to demonstrate that our results using 23 years of data are consistent with the trend found by Kasper et al. (2007) for a two year interval surrounding solar minimum 23.

In Section 7, we discuss how the demonstrated phase delay or hysteresis effect is qualitatively similar to the phase delays between SSN and many regularly observed solar indices (Ramesh & Vasantharaju 2014, and references therein). We note that the two aforementioned phase delays (τ_{slow} and τ_{fast}) are consistent with $L\alpha$ and SXR and that this consistency is indicative of two distinct source regions. Slower wind ($v_{\text{sw}} < 375 \text{ km s}^{-1}$) with a lower A_{He} originates in the streamer belt and responds to changes in SSN with characteristic delay time $\tau_{\text{slow}} = 150$ days. Faster wind with a larger A_{He} originates in ARs and responds to changes in SSN with characteristic delay time $\tau_{\text{fast}} > 300$ days. These different delay times indicate that A_{He} is processed by one or more mechanisms above the photosphere. Assuming that the results of Kasper et al. (2007) apply across the solar cycle and helium universally vanishes from the solar wind when $v_{\text{sw}} < 259 \text{ km s}^{-1}$ irrespective of solar activity, one possible interpretation is that there is a minimum A_{He} necessary for solar wind formation, the mechanisms that reduces A_{He} to a value less than its photospheric value prevents solar wind release below the vanishing speed v_0 , and—using the fit from Panel (b) of Fig. 2—any helium that enters the solar wind is released after 68 days, approximately two Carrington rotations. If this is the case, helium in the high-speed solar wind may represent the solar wind's "ground state" (Bame et al. 1977; Schwenn 2006) and the observed depletion of A_{He} is the result of source regions departing from states that release fast wind, i. e. those magnetically open to the heliosphere. A rigorous study of the relationship between A_{He} and solar indices other than SSN may better constrain helium variation by source region and is a subject of future work.

This work highlights the value of recent and forthcoming advances in heliophysics. Parker Solar Probe (Fox et al. 2016, PSP) launched in August, 2018 and completed its first perihelion in November of that year. Solar Orbiter (Müller et al. 2013, SoLO) will launch in 2020. The thermal ion instruments on board (Kasper et al. 2016) provide an unprecedented opportunity to study the solar wind, its formation, and its acceleration. For example, PSP will make measurements near and below the Alfvén critical point, i.e. at distances within which mapping the solar wind to specific sources is significantly simplified in comparison with *Wind*. McMullin et al. (2016) anticipate that the Daniel K. Inouye Solar Telescope (DKIST) will begin operations in 2020. DKIST’s Cryo-NIRSP instrument will be capable of simultaneously imaging solar helium at various heights

in the corona. Combining DKIST measurements with PSP and SoLO measurements will enhance our ability to differentiate between the mechanisms releasing helium into the solar wind—e.g. from the streamer belt or ARs—and better constrain the delay in helium’s response to changes in SSN.

This work was funded by NASA grants NNX17AI18G and 80NSSC18K0986. We are grateful to Michael Stevens for supplying the data and the referee for insightful comments. We also thank Lennard Fisk, Enrico Landi, Liang Zhao, Phyllis Whittlesey, and Michael Stevens for fruitful discussions.

Software: IPython (Perez & Granger 2007), Jupyter (Kluyver et al. 2016), Matplotlib (Hunter 2007), Numpy (vanderWalt et al. 2011), Pandas (McKinney 2010), Python (Oliphant 2007; Millman & Aivazis 2011)

REFERENCES

- Aellig, M. R., Lazarus, A. J., & Steinberg, J. T. 2001, *Geophysical Research Letters*, 28, 2767. <http://doi.wiley.com/10.1029/2000GL012771>
- Alterman, B. L., Kasper, J. C., Stevens, M. L., & Koval, A. 2018, *The Astrophysical Journal*, 864, 112. <http://dx.doi.org/10.3847/1538-4357/aad23f>
<http://stacks.iop.org/0004-637X/864/i=2/a=112?key=crossref.70d30c5e4f4e09560b242739d2b64fbc>
- Asplund, M., Grevesse, N., Sauval, A. J., & Scott, P. 2009, *Annual Review of Astronomy and Astrophysics*, 47, 481
- Bachmann, K. T., & White, O. R. 1994, *Solar Physics*, 150, 347. <http://link.springer.com/10.1007/BF00712896>
- Bame, S. J., Asbridge, J. R., Feldman, W. C., & Gosling, J. T. 1977, *Journal of Geophysical Research*, 82, 1487. <http://doi.wiley.com/10.1029/JA082i010p01487>
- Benz, A. O. 2008, *Living Rev. Solar Phys*, 5, 1. <http://www.livingreviews.org/lrsp-2008-1>
<http://www.astro.phys.ethz.ch/staff/benz/benz%5Cnhttp://creativecommons.org/licenses/by-nc-nd/2.0/de/>
- Borrini, G., Gosling, J. T., Bame, S. J., Feldman, W. C., & Wilcox, J. M. 1981, *Journal of Geophysical Research: Space Physics*, 86, 4565. <http://doi.wiley.com/10.1029/JA086iA06p04565>
- Eselevich, M. V., & Eselevich, V. G. 2006, *Astronomy Reports*, 50, 748
- Feldman, U., Landi, E., & Schwadron, N. A. 2005, *Journal of Geophysical Research: Space Physics*, 110, 1
- Feldman, W. C., Asbridge, J. R., Bame, S. J., & Gosling, J. T. 1978, *Journal of Geophysical Research*, 83, 2177
- Fisk, L. A. 2003, *Journal of Geophysical Research*, 108, 1157. <http://doi.wiley.com/10.1029/2002JA009284>
- Fontenla, J. M., Avrett, E. H., & Loeser, R. 2001, 636. <http://arxiv.org/abs/astro-ph/0109416>
<http://dx.doi.org/10.1086/340227>
- Fontenla, J. M., Reichmann, E. J., & Tandberg-Hanssen, E. 1988, *The Astrophysical Journal*, 329, 464. <http://adsabs.harvard.edu/doi/10.1086/166392>
- Fox, N. J., Velli, M. C., Bale, S. D., et al. 2016, *Space Science Reviews*, 204, 7. <http://link.springer.com/10.1007/s11214-015-0211-6>
- Goelzer, M. L., Smith, C. W., Schwadron, N. A., & McCracken, K. G. 2013, *Journal of Geophysical Research: Space Physics*, 118, 7525
- Hirshberg, J. 1973, *Reviews of Geophysics*, 11, 115. <http://doi.wiley.com/10.1029/RG011i001p00115>
- Hunter, J. D. 2007, *Computing in Science & Engineering*, 9, 90. <http://ieeexplore.ieee.org/document/4160265>
<http://ieeexplore.ieee.org/lpdocs/epic03/wrapper.htm?arnumber=4160265>
- Kasper, J. C., Lazarus, A. J., & Gary, S. P. 2008, *Physical Review Letters*, 101, 261103. <http://link.aps.org/doi/10.1103/PhysRevLett.101.261103>
- Kasper, J. C., Lazarus, A. J., Steinberg, J. T., Ogilvie, K. W., & Szabo, A. 2006, *Journal of Geophysical Research*, 111, A03105. <http://doi.wiley.com/10.1029/2005JA011442>

- Kasper, J. C., Stevens, M. L., Korreck, K. E., et al. 2012, *The Astrophysical Journal*, 745, 162.
<http://stacks.iop.org/0004-637X/745/i=2/a=162?key=crossref.3243440b8824f281eaf92619ea6e90c4>
- Kasper, J. C., Stevens, M. L., Lazarus, A. J., Steinberg, J. T., & Ogilvie, K. W. 2007, *The Astrophysical Journal*, 660, 901.
<http://stacks.iop.org/0004-637X/660/i=1/a=901>
- Kasper, J. C., Abiad, R., Austin, G., et al. 2016, *Space Science Reviews*, 204, 131.
<http://link.springer.com/10.1007/s11214-015-0206-3>
- Kasper, J. C., Klein, K. G., Weber, T., et al. 2017, *The Astrophysical Journal*, 849, 126.
<http://stacks.iop.org/0004-637X/849/i=2/a=126?key=crossref.a4fda357a12d19fd2ad1aa8a3897c78f>
- Kluyver, T., Ragan-kelley, B., Pérez, F., et al. 2016, *Positioning and Power in Academic Publishing: Players, Agents and Agendas*, 87
- Laming, J. M. 2004, *The Astrophysical Journal*, 614, 1063.
<http://adsabs.harvard.edu/abs/2004ApJ...614.1063L>
- . 2015, *Living Reviews in Solar Physics*, 12, doi:10.1007/lrsp-2015-2
- Laming, J. M., & Feldman, U. 2003, *The Astrophysical Journal*, 591, 1257
- Maruca, B. A., & Kasper, J. C. 2013, *Advances in Space Research*, 52, 723.
<http://dx.doi.org/10.1016/j.asr.2013.04.006>
- Mauas, P. J. D., Andretta, V., Falchi, A., et al. 2005, *The Astrophysical Journal*, 619, 604
- Mckinney, W. 2010, in *Proceedings of the 9th Python in Science Conference*, ed. S. van der Walt & J. Millman, 51 – 56
- McMullin, J. P., Rimmele, T. R., Warner, M., et al. 2016, 99061B. <http://proceedings.spiedigitallibrary.org/proceeding.aspx?doi=10.1117/12.2235227>
- Meyer, J. P. 1991, *Advances in Space Research*, 11, 269
- . 1993, *Advances in Space Research*, 13, 377
- Millman, K. J., & Aivazis, M. 2011, *Computing in Science & Engineering*, 13, 9.
<http://ieeexplore.ieee.org/document/5725235/>
- Müller, D., Marsden, R. G., St. Cyr, O. C., & Gilbert, H. R. 2013, *Solar Physics*, 285, 25
- Ogilvie, K. W., Chornay, D. J., Fritzenreiter, R. J., et al. 1995, *Space Science Reviews*, 71, 55.
<http://link.springer.com/10.1007/BF00751326>
- Oliphant, T. E. 2007, *Computing in Science & Engineering*, 9, 10. <http://ieeexplore.ieee.org/document/4160250/>
- Özgüç, A., & Ataç, T. 2001, in *IAU Symposium*, Vol. 203, *Recent Insights into the Physics of the Sun and Heliosphere: Highlights from SOHO and Other Space Missions*, ed. P. Brekke, B. Fleck, & J. B. Gurman, 125.
<http://adsabs.harvard.edu/abs/2001IAUS..203..125O>
- Perez, F., & Granger, B. E. 2007, *Computing in Science & Engineering*, 9, 21.
<http://ieeexplore.ieee.org/document/4160251/>
- Rakowski, C. E., & Laming, J. M. 2012, *The Astrophysical Journal*, 754, 65
- Ramesh, K. B., & Vasantharaju, N. 2014, *Astrophysics and Space Science*, 350, 479
- Schwadron, N. A., Fisk, L. A., & Zurbuchen, T. H. 1999, *The Astrophysical Journal*, 521, 859
- Schwenn, R. 2006, *Space Science Reviews*, 124, 51
- SILSO World Data Center. 2018
- Stakhiv, M., Lepri, S. T., Landi, E., Tracy, P., & Zurbuchen, T. H. 2016, *The Astrophysical Journal*, 829, 117. <http://stacks.iop.org/0004-637X/829/i=2/a=117?key=crossref.b0b55b70491e273f167cae33b403f34c>
- Temmer, M., Veronig, A., & Hanslmeier, A. 2003, *Solar Physics*, 215, 111
- van der Walt, S., Colbert, S. C., & Varoquaux, G. 2011, *Computing in Science & Engineering*, 13, 22.
<http://ieeexplore.ieee.org/document/5725236/>
- van Driel-Gesztelyi, L., & Green, L. M. 2015, *Living Reviews in Solar Physics*, 12, 1.
<http://link.springer.com/10.1007/lrsp-2015-1>
- Vanlommel, P., Cugnon, P., Van Der Linden, R. A. M., Berghmans, D., & Clette, F. 2005, *Solar Physics*, 224, 113
- Vauclair, S., & Charbonnel, C. 1991, in *Challenges to Theories of the Structure of Moderate-Mass Stars* (Berlin, Heidelberg: Springer Berlin Heidelberg), 37–41.
http://link.springer.com/10.1007/3-540-54420-8_48